Angewandte Chemie
Eine Zeitschrift der Gesellschaft Deutscher Chemiker

Supporting Information

69451 Weinheim, Germany

Probing Slow Chemical Exchange at Carbonyl Sites in Proteins by Chemical Exchange Saturation Transfer NMR Spectroscopy**

Pramodh Vallurupalli and Lewis E. Kay**

anie_201209118_sm_miscellaneous_information.pdf

Supporting Information

S1 NMR Spectroscopy:

Experimental Details for the Pulse Sequence of Figure 1: ^{1}H and ^{15}N carriers are placed on the water resonance and at 119 ppm, respectively, while the ^{13}C carrier is positioned at 176.5 ppm for the duration of the experiment, except between points *a* and *b* when it is shifted to the desired offset. A series of 2D planes (typically between 60-100) are recorded, each with a different offset of the CEST field. All ^{1}H pulses are applied at the highest power level, with the exception of the water selective 90° pulse at the start of the sequence (~1.5 ms rectangular pulse), the 6 kHz WALTZ-16$_x$ decoupling field and the flanking 90° pulses (of phase ±y). The ^{13}C rectangular pulses are applied at the highest power level, with the exception of the pulse pair before the CEST period that select for ^{13}CO magnetization where a field strength of $\Delta/\sqrt{15}$ [1] is used (Δ is the difference in Hz between the centers of the ^{13}CO and ^{13}Cα spectra; high power pulses could have been used instead). Typically ^{13}CO CEST fields range from 20-50 Hz, while ^{13}Cα decoupling is carried out using a 120.5 ppm cosine modulated SEDUCE-1 scheme[2] with a maximum amplitude of 3.14 kHz (11.7 T). ^{13}C shaped pulses of 450 μs (at 11.7T) with a profile that has been described previously[3] are used during the ^{15}N→^{13}CO CPMG-INEPT[4] transfer. Here the phases of each of the 32 ^{13}C and ^{15}N pulses are set according to the XY-16 scheme[5, 6] $\{x,y,x,y,y,x,y,x,-x,-y,-x,-y,-y,-x,-y,-x\}_2$ such that x is the phase of the first pulse, y is the phase of the second pulse and so forth. ^{15}N pulses were applied at the highest power level with the exception of those used for the ^{15}N→^{13}CO transfer where the power was reduced by 1-2 dB. A 1kHz ^{15}N WALTZ-16 decoupling field[7] was employed for detection. The following phase cycling was used: $\phi1=\{x,-x\}$, $\phi2=\{x\}$, $\phi3=\{x,x,-x,-x\}$, $\phi4=\{x\}$, receiver=$\{x,-x\}$. $\phi2$ and the receiver phase are incremented by 180° for each complex point[8]. Quadrature detection[9-11] in the indirect dimension was obtained using the gradient-sensitivity enhanced approach by recording a pair of data sets for each t_1 point with ($\phi4$,g6) and (-$\phi4$,-g6).[10, 11] Delays used were τ_a= 2.3 ms, τ_b= 2.75 ms, T= 10 ms, T_N= 14 ms and δ= 0.5 ms. A reference plane is recorded with T_{EX} set to

0, with the remaining data sets recorded with T_{EX} values on the order of 300-500 ms. χ_1 and χ_2 are set to max(0, T_N-t_1/2) and max(0, t_1/2-T_N) respectively[12]. Gradient strengths in G/cm (duration in ms) are g1 8 (0.5), g2 4 (0.5), g3 10 (1.0), g4 -7 (1.0), g5 -6 (0.6), g6 30 (1.25), g7 4 (0.3), g8 2 (0.4), g9 29.5 (0.125).

Experimental Details: The nutation method proposed by Guenneugues et al[13] was used in a 1D manner to calibrate the B_1 field applied during the CEST period (T_{EX} delay) of the scheme of Figure 1[14]. To avoid complications arising from evolution due to scalar couplings, for example ^{13}CO-^{15}N and ^{13}CO-$^{13}C^{\alpha}$ couplings in the case of the ^{13}CO CEST experiment, the B_1 field was calibrated at a value of 200-300 Hz. The lower B_1 fields used in the CEST experiments were then estimated assuming that the amplifier behaves linearly in the regime of interest (this has been verified).

A pair of ^{15}N CEST experiments were performed as described previously[14], with weak B_1 fields of 21.5 and 34.8 Hz. For B_1 = 21.5 (34.8) Hz, 75 (60) 2D ^{1}H-^{15}N spectra, T_{EX}=0.35 s, were recorded with the weak B_1 field applied at offsets equally spaced between 104.2 and 133.8 ppm (one offset per spectrum). A reference data set was recorded with T_{EX}=0. Each spectrum was recorded with 30 complex t_1 points (sweep width of 18.3 ppm), 8 transients/FID and a recycle delay of 1.5 s for total measurement times of 20.3 (B_1 = 21.5 Hz) and 16.3 (B_1 = 34.8 Hz) hours.

Four ^{13}CO CEST experiments were recorded using B_1 fields of 21.3, 34.6, 42.6 and 53.3 Hz. Each of the CEST data sets comprised 76, 61, 46 and 41 planes, respectively, with the CEST fields equally spaced between 170.6 and 182.5 ppm. T_{EX} was set to 0.3 s. ^{1}H-^{15}N data sets with 30 complex t_1 points, recycle delay = 1.5 s, twelve transients/FID were recorded leading to experimental times between 30 and 16.5 hours for each CEST series (depending on the number of 2D planes).

S2 Data Processing and Analysis:

Data Processing: NMR data were processed with NMRpipe[15] and visualized using SPARKY[16]. Peak intensities were quantified using FuDA (http://pound.med.utoronto.ca/software.html). Errors in the CEST 1D profiles were estimated as described earlier[14].

Data Analysis: All CEST data were analyzed using ChemEx (available upon request) that propagates a Bloch-McConnell[17] Louvillian to simulate the experiment and minimizes a standard χ^2 equation to obtain the best-fit parameters. In the case of 2S fits of ^{15}N CEST data, x,y,z components of magnetization were evolved for both the ground and excited states, as described previously[14]. Fitting parameters were: global parameters k_{ex}, p_E and residue specific ϖ_G, $\Delta\varpi_{GE}$, R_1, R_{2G}, R_{2E} and I_0. Here the ^{15}N longitudinal relaxation rate, R_1, is assumed to be the same for a spin in either G or E states, R_{2G} and R_{2E} are the ^{15}N transverse relaxation rates in the two states and I_0 is the initial intensity that differs for each experiment (*ie*, for each data set with a different weak B_1 CEST field). In the case of ^{13}CO CEST experiments x,y,z components of magnetization were evolved for each of the two ^{13}CO lines corresponding to spin-state 'up' or 'down' of the adjacent ^{13}Cα for both G and E states (12 components). Values of $\Delta\varpi$ and relaxation rates were assumed to be the same for both lines and $^1J_{C\alpha CO}$ was set to 51 Hz, so that the same number of fitting parameters was used as for ^{15}N CEST. Global fits of ^{15}N CEST data included 15 residues with $\Delta\varpi > 4$ ppm while the corresponding fits of ^{13}CO CEST data were based on 9 residues with $\Delta\varpi > 2$ ppm. Chemical shift differences for all other residues were obtained by performing single residue fits with k_{ex} and p_E fixed to values optimized from global fits.

Three-state fits of ^{15}N CEST data sets were also performed. Here the x,y,z magnetization components for each of the three states were evolved. Fitting parameters were: global parameters $k_{ex,FI}$, $k_{ex,IU}$, p_F and p_I ($p_U = 1 - p_F - p_I$) and residue specific parameters ϖ_F, $\Delta\varpi_{FI}$, $\Delta\varpi_{FU}$, R_1, R_2 and I_0. It has been assumed that the relaxation properties of all states are identical. A global fit was performed using 24 residues satisfying the criteria $\Delta\varpi > 2.5$ ppm (based on a 2S fit), using data recorded at 11.7 and 18.8 T.

Monte Carlo error estimates of parameters were obtained from analyses of 'in silico' generated data[18]. 200 CEST profiles were constructed from the best-fit parameters, including the addition of random noise at a level that corresponds to what is observed experimentally. Each of the 200 data sets is subsequently fit and 1 standard deviation of the extracted fitted parameters is defined as the error.

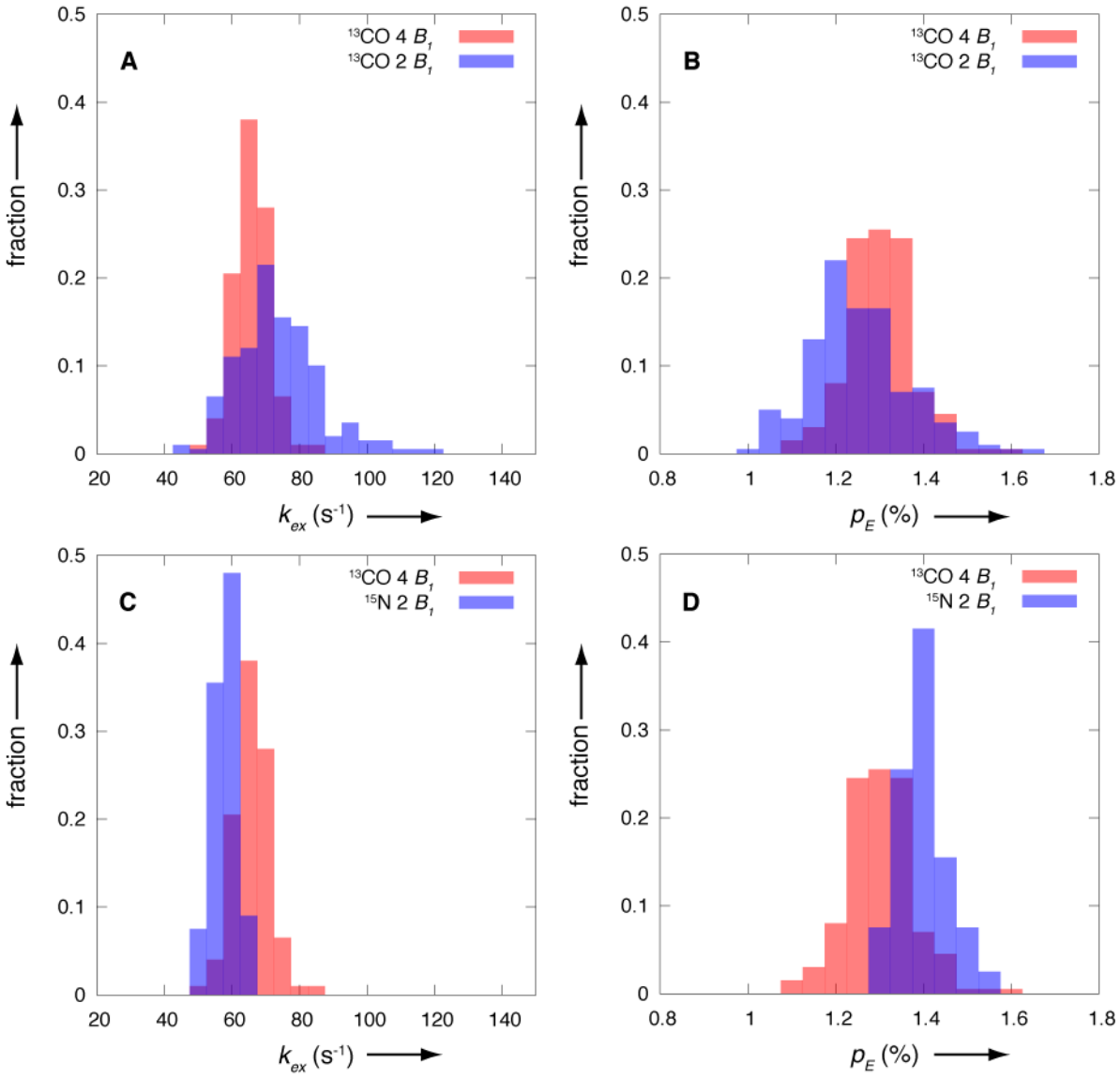

Figure S1: Monte Carlo analysis shows that the exchange parameters obtained from fits of ^{13}CO and ^{15}N CEST data sets are similar. Distribution of k_{ex} (A,C) and p_E (B,D) values. (A,B) Fits of CEST data recorded at four different B_1 fields, instead of two, reduces the spread in parameters. (C,D) The overlap in fitting parameters obtained using ^{15}N and ^{13}CO CEST data establish that the ^{15}N and ^{13}CO experiments are self-consistent. The histograms contain data from 200 Monte Carlo simulations.

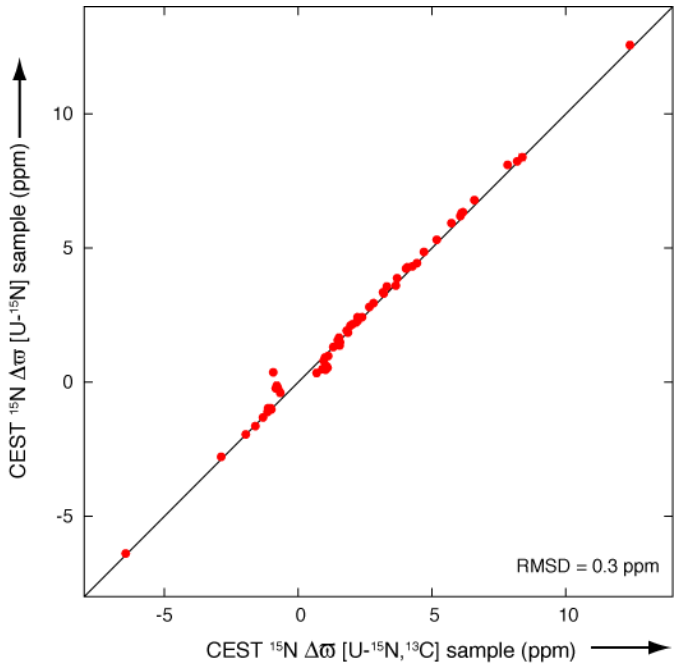

Figure S2: Correlation between extracted $\Delta\varpi$ values from ^{15}N CEST experiments recorded on A39G FF using [U-^{15}N] (y axis) and [U-^{15}N,^{13}C] (x axis) samples, 1ºC. Note that the unresolved $^{1,2}J_{N,C}$ couplings in data sets recorded on the [U-^{15}N,^{13}C] sample have not been taken into account in analysis of the data. An RMSD of 0.3 ppm is obtained, which reduces to 0.2 ppm when residues with $\Delta\varpi < 1$ ppm are excluded.

Table S1: Backbone amide ^{15}N and ^{13}CO $\Delta\varpi$ values obtained from a two state analysis of CEST data recorded on a [U-^{15}N,^{13}C] sample of A39G FF, 1°C. Single residue fits with k_{ex} and p_E fixed to the best-fit values (see above) were performed to obtain the listed $\Delta\varpi$ values. Errors were generated by a covariance matrix analysis[18].

Residue	^{15}N		^{13}CO	
	$\Delta\varpi$ (ppm)	error	$\Delta\varpi$ (ppm)	error
01	----	----	----	----
02	----	----	0.24	0.05
03	----	----	----	----
04	----	----	0.33	0.04
05	----	----	0.22	0.04
06	----	----	-0.36	0.02
07	----	----	0.42	0.03
08	-1.13	0.05	0.45	0.04
09	-0.76	0.05	0.74	0.04
10	1.53	0.05	1.21	0.05
11	1.55	0.10	0.68	0.03
12	0.89	0.06	-0.02	0.05
13	4.08	0.04	0.30	0.05
14	-0.84	0.05	-0.95	0.03
15	1.81	0.03	-1.38	0.03
16	1.30	0.05	-1.47	0.03
17	-1.14	0.05	-0.26	0.05
18	2.02	0.04	-1.05	0.03
19	1.12	0.05	-0.99	0.03
20	1.09	0.06	0.28	0.07
21	0.99	0.08	-0.68	0.03
22	3.17	0.04	-1.03	0.03
23	-0.80	0.07	-1.04	0.03
24	-0.68	0.09	1.82	0.02
25	2.66	0.04	0.87	0.03
26	5.18	0.03	-3.58	0.02
27	-1.95	0.04	-2.61	0.03
28	6.58	0.05	1.63	0.02
29	5.73	0.04	0.32	0.06
30	1.47	0.06	----	----
31	----	----	-0.36	0.04
32	-0.93	0.05	0.64	0.02
33	4.26	0.03	-0.85	0.02
34	0.95	0.03	0.25	0.05
35	-1.31	0.04	-0.74	0.03
36	0.69	0.08	0.95	0.03
37	4.70	0.03	-1.61	0.02
38	2.38	0.03	-1.57	0.03
39	1.56	0.04	0.19	0.08
40	-1.02	0.05	0.17	0.08
41	6.05	0.03	-1.07	0.03
42	6.12	0.04	-1.07	0.04
43	12.40	0.07	0.79	0.03
44	3.31	0.06	1.34	0.02
45	3.69	0.03	0.27	0.04
46	1.02	0.04	----	----
47	----	----	-0.92	0.03
48	2.21	0.03	----	----
49	----	----	-0.21	0.05
50	8.18	0.03	1.22	0.02
51	1.52	0.04	2.15	0.07
52	8.37	0.11	3.45	0.01
53	-2.88	0.03	-0.17	0.04
54	3.18	0.03	0.15	0.12
55	-6.45	0.02	-0.77	0.03
56	3.66	0.04	-2.57	0.03
57	1.07	0.05	-2.37	0.02
58	1.00	0.06	-1.18	0.03
59	6.16	0.03	-1.89	0.02
60	2.22	0.03	-3.04	0.02
61	2.17	0.03	-2.25	0.02

62	-1.02	0.04	-0.83	0.02
63	2.81	0.03	-3.09	0.02
64	1.95	0.03	-2.42	0.02
65	-1.60	0.04	-1.79	0.03
66	4.02	0.03	-1.96	0.02
67	7.83	0.02	----	----
68	4.43	0.02	----	----
69	1.87	0.03	----	----

Table S2: Backbone amide ^{15}N $\Delta\varpi_{FI}$ and $\Delta\varpi_{FU}$ values obtained by a three state analysis of the ^{15}N CEST data recorded on a [U-^{15}N] sample of A39G FF, 1ºC. Errors were obtained by a covariance matrix analysis[18].

Residue	**$\Delta\varpi_{FI}$(ppm)**	**Error**	**$\Delta\varpi_{FU}$(ppm)**	**Error**
13	0.50	0.14	4.92	0.02
22	0.76	0.10	3.85	0.01
25	0.28	0.10	3.28	0.01
26	2.45	0.09	5.85	0.01
28	1.54	0.21	7.49	0.02
29	1.45	0.17	6.60	0.02
33	1.62	0.09	4.84	0.01
37	1.61	0.11	5.42	0.01
41	2.78	0.11	6.80	0.01
42	1.71	0.18	6.98	0.02
43	7.10	0.20	13.31	0.02
44	-1.42	0.19	4.24	0.02
45	-0.68	0.17	4.54	0.02
50	5.71	0.08	8.72	0.01
52	7.25	0.06	8.65	0.01
53	-4.71	0.07	-2.37	0.01
54	0.99	0.08	3.77	0.01
55	-7.81	0.06	-6.07	0.01
56	5.57	0.07	3.19	0.01
59	4.58	0.07	6.70	0.01
63	1.59	0.07	3.25	0.01
66	2.74	0.08	4.55	0.01
67	6.56	0.06	8.45	0.01
68	2.96	0.06	4.75	0.01

References

[1] L. E. Kay, M. Ikura, R. Tschudin, A. Bax, *J Magn Reson* **1990**, *89*, 496.

[2] M. A. Mccoy, L. Mueller, *J Am Chem Soc* **1992**, *114*, 2108.

[3] P. Lundstrom, D. F. Hansen, L. E. Kay, *J Biomol NMR* **2008**, *42*, 35.

[4] L. Mueller, P. Legault, A. Pardi, *J Am Chem Soc* **1995**, *117*, 11043.

[5] T. Gullion, D. B. Baker, M. S. Conradi, *J Magn Reson* **1990**, *89*, 479.

[6] V. Y. Orekhov, D. M. Korzhnev, L. E. Kay, *J Am Chem Soc* **2004**, *126*, 1886.

[7] A. J. Shaka, J. Keeler, T. Frenkiel, R. Freeman, *J Magn Reson* **1983**, *52*, 335.

[8] D. Marion, M. Ikura, R. Tschudin, A. Bax, *J Magn Reson* **1989**, *85*, 393.

[9] A. G. Palmer, J. Cavanagh, P. E. Wright, M. Rance, *J Magn Reson* **1991**, *93*, 151.

[10] L. E. Kay, P. Keifer, T. Saarinen, *J Am Chem Soc* **1992**, *114*, 10663.

[11] J. Schleucher, M. Sattler, C. Griesinger, *Angew Chemie Int Ed* **1993**, *32*, 1489.

[12] J. F. Ying, J. H. Chill, J. M. Louis, A. Bax, *J Biomol NMR* **2007**, *37*, 195.

[13] M. Guenneugues, P. Berthault, H. Desvaux, *J Magn Reson* **1999**, *136*, 118.

[14] P. Vallurupalli, G. Bouvignies, L. E. Kay, *J Am Chem Soc* **2012**, *134*, 8148.

[15] F. Delaglio, S. Grzesiek, G. W. Vuister, G. Zhu, J. Pfeifer, A. Bax, *J Biomol NMR* **1995**, *6*, 277.

[16] T. D. Goddard, D. G. Kneller, *SPARKY 3 University of California, San Francisco*.

[17] H. M. McConnell, *J Chem Phys* **1958**, *28*, 430.

[18] W. H. Press, B. P. Flannery, S. A. Teukolsky, W. T. Vetterling, *Numerical Recipes in C. The Art of Scientific Computing* Second Edition ed., Cambridge University Press, Cambridge (UK), **1992**.